



**HAL**  
open science

## Acoustic cloaking: Geometric transform, homogenization and a genetic algorithm

Lucas Pomot, Cédric Payan, Marcel Remillieux, Sebastien Guenneau

### ► To cite this version:

Lucas Pomot, Cédric Payan, Marcel Remillieux, Sebastien Guenneau. Acoustic cloaking: Geometric transform, homogenization and a genetic algorithm. *Wave Motion*, 2020, 92, pp.102413. 10.1016/j.wavemoti.2019.102413 . hal-02399059

**HAL Id: hal-02399059**

**<https://hal.science/hal-02399059>**

Submitted on 20 Jul 2022

**HAL** is a multi-disciplinary open access archive for the deposit and dissemination of scientific research documents, whether they are published or not. The documents may come from teaching and research institutions in France or abroad, or from public or private research centers.

L'archive ouverte pluridisciplinaire **HAL**, est destinée au dépôt et à la diffusion de documents scientifiques de niveau recherche, publiés ou non, émanant des établissements d'enseignement et de recherche français ou étrangers, des laboratoires publics ou privés.



Distributed under a Creative Commons Attribution - NonCommercial 4.0 International License

# Acoustic cloaking: geometric transform, homogenization and a genetic algorithm

Lucas Pomot<sup>1,3</sup>, Cédric Payan<sup>1</sup>, Marcel Remillieux<sup>2</sup>, Sébastien Guenneau<sup>3</sup>

---

## Abstract

A general process is proposed to experimentally design anisotropic inhomogeneous metamaterials obtained through a change of coordinates in the Helmholtz equation. The method is applied to the case of a cylindrical transformation that allows cloaking to be performed. To approximate such complex metamaterials we apply results of the theory of homogenization and combine them with a genetic algorithm. To illustrate the power of our approach, we design three types of cloaks composed of isotropic concentric layers structured with three types of perforations: curved rectangles, split rings and crosses. These cloaks have parameters compatible with existing technology and they mimic the behavior of the transformed material. Numerical simulations have been performed to qualitatively and quantitatively study the cloaking efficiency of these metamaterials.

*Keywords:* Cloaking, homogenization, genetic algorithm, geometric transform, machine learning

---

## 1. Introduction

The geometrical transformation of Maxwell's equations has been studied theoretically back in 1962 by Post [1] and numerically solved with a finite element method in 1994 by Nicolet *et al.* [2] and with a finite-difference time-domain  
5 method in 1996 by Ward and Pendry [3], among others. These works were

---

<sup>1</sup>Aix Marseille Univ, CNRS, Centrale Marseille, LMA, Marseille, France

<sup>2</sup>Geophysics Group (EES-17), Los Alamos National Laboratory, Los Alamos, New Mexico 87545, USA

<sup>3</sup>Aix Marseille Univ, CNRS, Centrale Marseille, Institut Fresnel, Marseille, France

primarily focused on the equations governing electromagnetism. More recently, Greenleaf *et al.* [4] (2003) mathematically established that specific geometric transformations, applied to the conductivity equation, lead to anisotropic heterogeneous conductivities giving rise to the same voltage and current measurements, at the boundary of a body, as an isotropic homogeneous conductivity. Such anisotropic conductivities, that cannot be detected by electrical impedance tomography, play a prominent role in cloaking devices whose purpose is to render an object invisible. Leonhardt [5] (2006) and Pendry *et al.* [6] (2006) showed that similar transformations can be used to perform cloaking on electromagnetic waves i.e. to guide light around some region, rendering it invisible over a certain frequency bandwidth. These results have inspired similar studies in acoustic waves which satisfy an equation of propagation analogous to that of electromagnetic waves. In acoustics, a geometrical transformation introduces either an anisotropic mass density (Cummer *et al.* [7] 2007, Chen *et al.* [8] 2007, Cummer *et al.* [9] 2008) or an anisotropic inertia (Milton *et al.* [10] 2007). Such medium properties can arise from microstructures as discussed in Mei *et al.* [11] (2007) and Torrent *et al.* [12] (2008). A challenge for any experimental application is then to find the appropriate microstructure that properly mimics the transformed parameters. In this article we propose a process to efficiently determine this microstructure. The article is organized as follows: after recalling some elementary results on geometrical transformations (Section 2) and homogenization (Section 3.1) in the context of the Helmholtz equation, we explain in Section 3.2 how a genetic algorithm can be used to design the microstructure associated with a given geometrical transformation. This process is illustrated in Section 4, which starts by a conformal mapping between Cartesian and polar coordinates (Section 4.1), which is combined with a non-linear transformation mapping a disc on an annulus; two cylindrical cloaks are then designed, with an alternation of isotropic homogeneous layers (Section 4.2) and same with elliptical perforations (Section 4.3); additional cloak's designs are also proposed with complex microstructures in Section 5; some of these microstructures seem to be more suited for experimental application as they require a smaller range of

elastic parameters. We finally discuss some perspectives on our work in Section 6.

## 2. Elementary results on geometrical transformation

In this section, we recall some elementary results on a geometrical transformation applied to a time-harmonic wave equation of the form:

$$\nabla \cdot a(\mathbf{X})\nabla u(\mathbf{X}) + b(\mathbf{X})\omega^2 u(\mathbf{X}) = 0 \quad (1)$$

with  $a$  and  $b$  the spatially varying parameters that describe the medium of propagation. This Helmholtz equation appears in various fields of physics such as acoustic propagation and electromagnetism. For instance, if we consider anti-plane shear waves propagating within a solid elastic medium invariant along the anti-plane direction, then  $a$  represents the shear modulus and  $b$  stands for the mass density of the medium [13]; likewise if we consider transverse magnetic waves in a dielectric medium invariant along the anti-plane direction,  $a$  gives the inverse of electric permittivity and  $b$  is the magnetic permeability [14]; if we consider water waves,  $a$  can stand for water depth, in which case  $b = 1$  [15], or  $a$  stands for the product of the phase and group density while  $b$  is then the ratio of the group and phase velocities in the context of the mild-slope equation [16]. Here, we choose to study pressure acoustic waves propagating within a non-viscous fluid, and so  $a$  is the inverse of mass density and  $b$  is the inverse of bulk modulus but our results can be easily translated to the fore mentioned wave areas. In the following  $a$  and  $b$  are supposed to be constant parameters.

We now apply a coordinate transformation of the form  $\phi : \mathbf{X} \rightarrow \mathbf{x}$  on the domain of propagation. Using results in [17] it is a straightforward matter to obtain the governing equation:

$$\nabla \cdot \alpha \nabla u(\mathbf{x}) + \beta \omega^2 u(\mathbf{x}) = 0 \quad (2)$$

where  $\alpha = aJ^{-1}J^{-T}\det J$  is now a matrix valued spatially varying parameter that depends on the Jacobian  $J_{ij} = \partial x_i / \partial X_j$  of the geometrical transformation  $\phi$  and where  $\beta = b \det J$  is a spatially varying scalar parameter.  $J^{-1}$  denotes the

inverse of  $J$  and  $J^{-T}$  the inverse of the transpose of  $J$ . Our main observation here is that the equation of propagation is form invariant meaning that the transformed equation still describes the same physical phenomena but not in the same medium of propagation. Let us focus our analysis on the following non-linear geometrical transformation which is written in polar coordinates:

$$\phi : \mathbf{X} \rightarrow (r, \theta) \rightarrow (r' = \sqrt{\frac{R_2^2 - R_1^2}{R_2^2} r^2 + R_1^2}, \theta' = \theta) \rightarrow \mathbf{x}. \quad (3)$$

This geometrical transformation introduces an annulus of anisotropic inhomogeneous material of internal radius  $R_1$  and external radius  $R_2$  (see figure 1b) in the propagation domain. In theory this transformation sends a point to a disk of radius  $R_1$ , however this approach introduces a divergence in the properties of the transformed medium. In practice it is thus preferable to send a disk of radius  $\epsilon$  very small in comparison with the other characteristic lengths onto a disk of radius  $R_1$ . If the initial disk of size  $\epsilon$  is composed of the same material as the surrounding medium we call this transformation non-linear Kohn's transformation. If the initial disk is empty, meaning it is a perforation in the medium of propagation with homogeneous Neumann boundary condition (i.e. zero normal derivative corresponding to zero flux at the boundary), we call the transformation non-linear Pendry's transformation. Let us note that such Neumann boundary conditions hold in our acoustic case for rigid cylinders [18], as well as in the water wave case [16]. However, this model holds for void cylindrical inclusions in the context of anti-plane shear waves, and infinite conducting cylinders for the context of transverse magnetic waves. From now on, we denote by perforations such types of inclusions. It is useful to consider three compound geometric transforms: first mapping Cartesian coordinates onto polar coordinates with Jacobian  $J_{xr} = \frac{\partial(r,\theta)}{\partial(x_1,x_2)}$ , then performing the transformation introduced in equation 3 with Jacobian  $J_{rr'} = \frac{\partial(r',\theta')}{\partial(r,\theta)}$  and finally mapping back from stretched polar coordinates to stretched Cartesian coordinates with Jacobian  $J_{r'x'} = \frac{\partial(x',y')}{\partial(r',\theta')}$ . The total Jacobian  $J_{xx'}$  and its determinant are given

by:

$$J_{xx'} = J_{xr} J_{rr'} J_{r'x'} \quad (4)$$

$$= R(\theta) \text{diag}(1, r) J_{rr'} \text{diag}(1, 1/r') R(\theta') \quad (5)$$

$$= R(\theta) \begin{bmatrix} \frac{r'}{R_2^2 - R_1^2} & 0 \\ \frac{r}{R_2^2} & \frac{r'}{r'} \end{bmatrix} R(\theta') \quad (6)$$

$$\det J = \frac{R_2^2}{R_2^2 - R_1^2} \quad (7)$$

$R(\theta)$  being the rotation matrix through an angle  $\theta$ . The main advantage of this non-linear geometrical transformation in comparison with Pendry's or Kohn's transformation is that the determinant of the Jacobian is constant thus the transformed medium parameter  $\beta = b \det J$  is constant. The new medium parameters derived from transformation (3) are

$$\alpha = a J^{-1} J^{-T} \det J = a R(-\theta') \begin{bmatrix} \frac{r'^2 - R_1^2}{r'^2} & 0 \\ 0 & \frac{r'^2}{r'^2 - R_1^2} \end{bmatrix} R(\theta') \quad (8)$$

$$\beta = b \det J = b \frac{R_2^2}{R_2^2 - R_1^2}. \quad (9)$$

$$(10)$$

40 We implement these anisotropic inhomogeneous medium parameters in COM-  
 SOL numerical simulation software. Results are shown in figure 1c, 1d. Control  
 of wave propagation achieved here could have several applications in various  
 fields of physics. However, considering the characteristics of the transformed  
 material, such medium would be difficult to create in practice. What we sug-  
 45 gest instead is to structure the medium of propagation on a microscopic level  
 (according to the field of physics that we consider) and to use classical re-  
 sults of homogenization theory to determine and tune effective properties of the  
 medium.

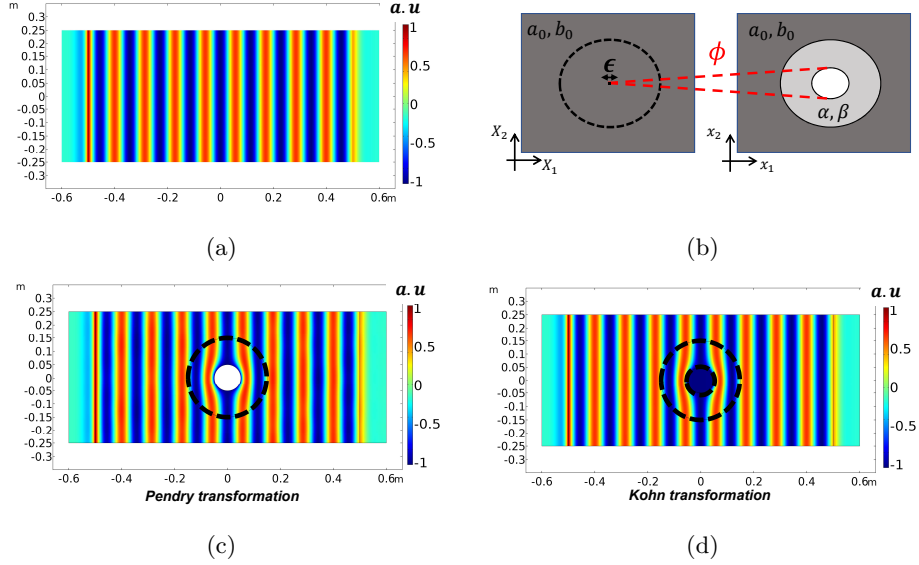


Figure 1: a) Propagation of a monochromatic wave from left to right in an homogeneous medium defined by  $a = 1$  and  $b = 4.45 \cdot 10^{-7}$  with PML at  $x = 0.5m$  and  $x = -0.5m$ . b) Schematic representation of geometrical transformation applied to an homogeneous medium sending a disk of radius  $\epsilon$  to a disk of radius  $R_{int}$ . c) and d) Numerical results obtained for both the non-linear Pendry's (c) and the non-linear Kohn's (d) transformation. The form invariant property of the equation of propagation is clearly visible as the wavefield is distorted only in the region affected by the transformation. Note the presence of perfectly matched layers on the left and right hand sides.

### 3. Inverse homogenization using a genetic algorithm

#### 50 3.1. Homogenization of the Helmholtz equation

In order to mimic these anisotropic inhomogeneous materials mathematically introduced in the previous section we apply classical results of homogenization theory in order to determine effective parameters of a complex medium with small perturbations. The aim of this approach is to perform what we wish to call an inverse homogenization (or retrieval method [19], [20], [15], [21]), where  
 55 characteristics of the small perforations are tuned to obtain an effective medium that corresponds to the medium given by the change of variable. Homogenization results used here were derived using asymptotic expansions as in [22] and

thus only the main results are recalled here for two different cases.

60 *Homogenization of a 1D laminar lattice*

A canonical example consists of an alternation of two isotropic propagation media (see figure 2a). Analytical formulae can then be deduced to determine properties of the effective anisotropic medium [22]:

$$\alpha = \begin{bmatrix} \langle a^{-1} \rangle^{-1} & 0 \\ 0 & \langle a \rangle \end{bmatrix} \quad (11)$$

$$\beta = \langle b \rangle$$

where  $\langle a \rangle = L_0 a_0 + L_1 a_1$ ,  $L_0$  and  $L_1$  being the thickness of the two layers that compose the microstructure (see figure 2a). In this configuration the tuning parameters are defined by the homogeneous isotropic media characterized by the parameters  $(a_i, b_i)$ ,  $i \in 0, 1$ . Possible additional tuning parameters are sizes  $L_0$  and  $L_1$  of layers. In the following numerical results we choose to set  $L_0 = L_1$ . To derive numerical values of  $a_1$  and  $a_2$  we solve the following system [23]:

$$\begin{cases} \alpha_{rr} = \langle a^{-1} \rangle^{-1} = \frac{a_0 a_1}{a_1 L_0 + a_0 L_1} \\ \alpha_{\theta\theta} = \langle a \rangle = L_0 a_0 + L_1 a_1 \\ \beta = \langle b \rangle = L_0 b_0 + L_1 b_1 \end{cases} \quad (12)$$

When  $L_0 = L_1 = 0.5$ , expressions for  $\alpha_{\theta\theta}$  and  $\alpha_{rr}$  reduce to:

$$\begin{cases} a_0 = \alpha_{\theta\theta} - \sqrt{\alpha_{\theta\theta}^2 - \alpha_{\theta\theta} \alpha_{rr}} \\ a_1 = \alpha_{\theta\theta} + \sqrt{\alpha_{\theta\theta}^2 - \alpha_{\theta\theta} \alpha_{rr}} \end{cases} \quad (13)$$

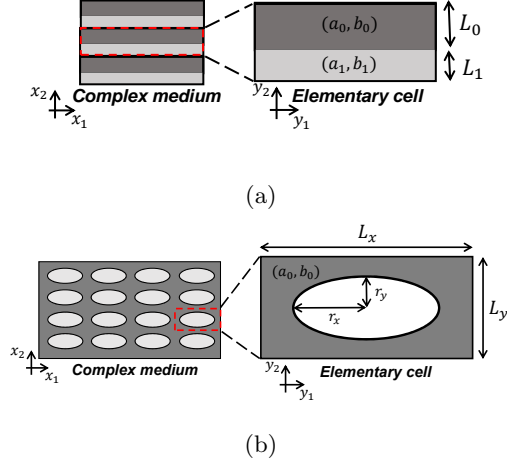


Figure 2: a) Schematic representation of 1D laminar lattice defined by 6 parameters if  $L_0 \neq L_1$  and 4 parameters if  $L_0 = L_1$ . b) Schematic representation of 2D periodic rectangular lattice defined by 6 parameters. We use those two lattices to mimic the desired medium through homogenization.

We note here that we can solve this system in the  $(r, \theta)$  domain if we then map the obtained microstructure to the  $(x, y)$  domain using a conformal map, a point we will develop in section (4.1). The only terms in this system of equations 13 that are dependent on the geometrical transformation are on the left hand side of the equations. Previously we justified the choice of our transformation (3) by arguing that the determinant of the associated Jacobian is constant and thus we have a constant  $\beta$ . However we did not take into account the influence of this transformation on values of the homogenized elastic parameters  $a_0$ ,  $a_1$ ,  $b_0$ ,  $b_1$ . Some transformations may be more suitable for experimental realizations depending on these homogenized elastic parameters they require. We discuss here values taken by such parameters for different transformations defined by:

$$\phi^n : (r, \theta) \rightarrow (r' = \left( \frac{R_2^n - R_1^n}{R_2^n} r^n + R_1^n \right)^{\frac{1}{n}}, \theta' = \theta) \quad (14)$$

where  $n$  is a positive integer.  $n = 1$  is the classic linear Pendry's transformation, and  $n = 2$  is the quadratic transformation defined in equation (3). We then compute parameters  $a_0(r')$  and  $a_1(r')$  for  $n = 1, 2, 3, 10$ . Results are

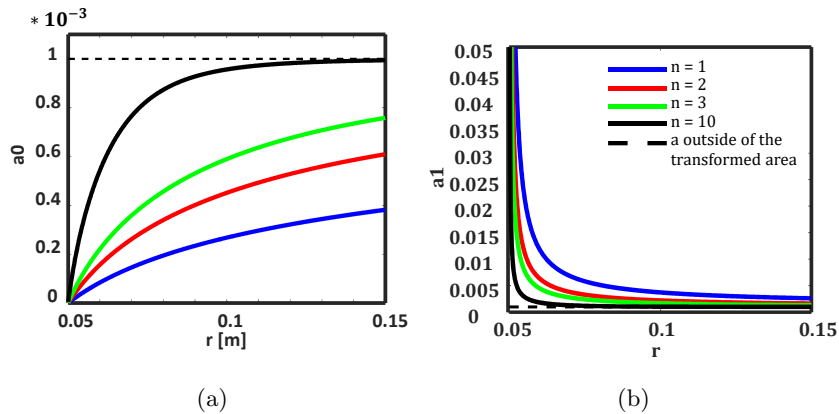


Figure 3: Variation of homogenized parameters  $a_0$  (a) and  $a_1$  (b) depending on the order  $n$  of the transformation. Note that the higher the order of the transformation the faster the homogenized parameters ( $a_0, a_1$ ) approach the parameter  $a$ . Note also the larger the variation for  $r$  close to  $R_{int}$ . Regarding experimental applications, the high order transformations should be considered when it is doable to create an intense and localized change in the properties of the medium propagation. On the other hand, if it is easier to create a slow gradient in the propagation medium properties one should consider a low order transformation.

65 shown in figure 3 and we observe that the homogenized parameters do not require the same variation for each order  $n$  of the transformation. This can be of paramount importance when considering experimental realization. In the following we consider the case  $n = 2$ . To choose parameters  $b_0$  and  $b_1$  we consider an under-determined system, meaning that we have an extra degree of freedom  
70 in their choice. The simplest solution would be to take  $b_0 = b_1 = \beta$  but depending on experimental realization this may not be the best choice as we will see in the sequel.

#### *Homogenization of a 2D periodic rectangular lattice*

We consider here a complex medium made of identical elementary cells regularly spaced, see figure 2b. This periodic structure is similar to that in [24], which proposes a combination of a geometric transformation, a homogenization theory called the Integral Equation method [25] and an optimization algorithm to design an acoustic metamaterial with an emphasis on perfect sound absorp-

tion at deep subwavelengths. In a similar way, to model this type of periodic medium we make use of two-scale homogenization theory [22] and for this purpose we introduce a microscopic scale described by the variable  $\mathbf{y}$  in addition to the macroscopic scale described by  $\mathbf{x}$ . The effective parameters of such a medium can be numerically calculated. We recall here the expressions of these effective parameters [22], [26]:

$$\alpha^H = \begin{bmatrix} \langle a \rangle - \langle a \partial_{y_1} w_1 \rangle & -\langle a \partial_{y_1} w_2 \rangle \\ -\langle \partial_{y_2} w_1 \rangle & \langle a \rangle - \langle a \partial_{y_2} w_2 \rangle \end{bmatrix} \quad (15)$$

$$\beta^H = \langle b \rangle$$

where  $\langle \cdot \rangle$  is the mean operator over an elementary cell,  $\partial_{y_i} w_j$  denotes the partial derivative of  $w_i$  with respect to  $y_j$  and  $(w_1, w_2)$  are the solutions defined up to an additional constant of the annex problem solved on only one elementary cell with periodic boundary conditions

$$\nabla_{\mathbf{y}} \cdot (a(\nabla_{\mathbf{y}} w_j(\mathbf{y}) + \mathbf{e}_j)) = 0 \quad (16)$$

with  $\mathbf{e}_1 = (1, 0)$  and  $\mathbf{e}_2 = (0, 1)$  the vectors of the basis. In this case the effective properties of the medium can be tuned using several parameters such as the perforation geometry (elliptical in our case), medium properties or the size of the elementary cell. All these parameters are described in figure 2b. Our objective is now to find the correct set of parameters that makes it possible to properly mimic the medium of propagation. We called this process inverse homogenization: we tune the elementary cell to obtain the desired homogenized medium of propagation. Considering the number of tuning parameters and the lack of completely analytical formula we implement a genetic algorithm that is well suited to solve such inverse problems.

### 3.2. Genetic algorithm

The inverse problem is solved using a genetic algorithm (GA) proposed in [27]. The main advantage of GA over other optimization process is its efficiency

to find a global minimum within a large and discrete solution space. In our case we try to minimize the following cost function:

$$\gamma(\alpha^H) = \max_{\{ij\}} \frac{|\alpha_{ij} - \alpha_{ij}^H|}{|\alpha_{ij}|} \quad (17)$$

for various sets of parameters defined in figure 2). In this formula  $\alpha$  defines the characteristics of the medium to be approximated and  $\alpha^H$  the homogenized medium for a particular set of parameters. The GA will be used to perform stochastic search based on the principles of natural selection and evolution.

90 An initial population  $N$  of individuals is generated, with each individual being defined by its set of parameters. For the initial iteration the parameters are chosen randomly. Homogenization is then performed for each set of parameters (meaning that we solve the annex problem for each set of parameters) and evaluated using the cost function  $\gamma$  defined in equation (17). The closer  
95 the homogenized medium to the desired medium, the smaller the cost function. Individuals who did poorly at this iteration are then eliminated and new sets of parameters are determined based on individuals that survived the previous iteration. Each parameter can be compared to a gene and the set of parameters to a DNA (which takes its name from biology). To determine the DNA of the  
100 next generation we take the arithmetic means of the parents' genes, meaning that if parent  $i$  is defined as  $p^i = \{a^i, b^i, L_x^i, L_y^j, r_x^i, r_y^i\} = DNA(p^i)$  and parent  $i + 1$  as  $p^{i+1} = DNA(p^{i+1})$ , then the genes of children  $c^i$  are defined as  $DNA(c^i) = \mu DNA(p^i) + (1 - \mu) DNA(p^{i+1})$  where  $\mu$  is an arbitrary real number between 0 and 1. To avoid being trapped in local minima we add a mutation  
105 factor which takes a chosen percentage of genes picked randomly and attribute them random values. Thus, if the algorithm converges to a minimum that is not a global minimum a random mutation can still create an individual with a better performing DNA. This individual can then influence further generations. There can be a lot of tweaking in GA to choose the ideal population number,  
110 mutation rate or other parameters that we did not introduce here for sake of simplicity. However the GA performed adequately in our case and allowed us to determine quickly a large number of elementary cells that properly mimic our

transformed medium after approximately 15 iterations.

115 **4. Illustrative numerical results**

4.1. *Conformal mapping*

In section 3.1 we quickly introduced the fact that the microstructures are designed in  $(r, \theta)$  coordinates whereas we want to obtain a final microstructure in  $(x, y)$  coordinates. In fact the inverse homogenization will take place in  $(r, \theta)$  coordinates before being mapped on  $(x, y)$  coordinates using a conformal map, a geometrical transformation that does not impact the medium properties. The conformal map we consider maps a rectangular domain  $[R_1, R_2] \times [-\pi/\eta, \pi/\eta]$  onto an annular domain  $[R_1, R_2] \times [0, 2\pi]$  [16]:

$$w = \psi e^{\eta(x+iy)}, \quad \text{with} \quad \eta = \frac{\ln(R_2/R_1)}{R_2 - R_1} \quad \psi = \frac{R_2 + R_1}{e^{\eta R_2} + e^{\eta R_1}} \quad (18)$$

It is important to note here that the medium given by the change of variable is inhomogeneous in addition to being anisotropic whereas homogenization theory can only achieve homogeneous anisotropic media. To achieve the required inhomogeneity we approximate the inhomogeneous anisotropic medium by several homogeneous anisotropic media. The impact of this approximation is quantitatively studied in figure 4. Based on these results we choose to divide our medium into  $M = 20$  homogeneous anisotropic media. However it is important to notice that this approximation can be effective for  $M = 5$ . A similar question arises when choosing the number  $N$  of elementary cells needed to properly describe a homogeneous anisotropic material. In our case we find that  $N = 3$  elementary cells for the laminar case and only  $N = 1$  elementary cell for the periodic rectangular lattice give quantitatively good results.

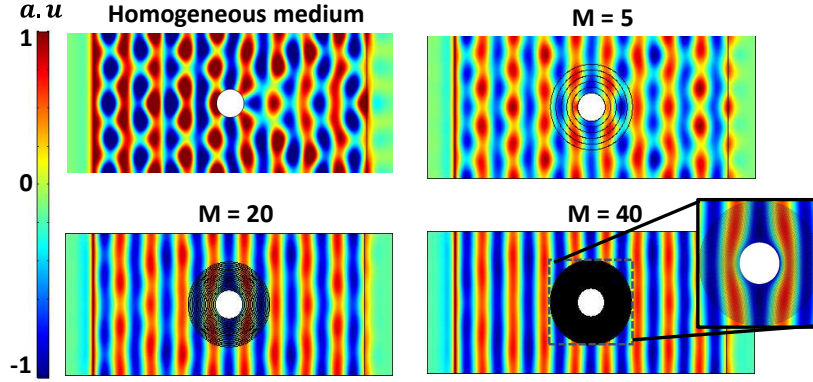


Figure 4: Qualitative results for various choices of subdivision  $M$  of the anisotropic inhomogeneous medium into anisotropic homogeneous medium. Note the visually good results obtained from  $M = 20$  but note also that  $M = 5$  gives already a noticeable reduction of scattering in comparison with the obstacle in the homogeneous medium.

130 *4.2. 1D laminar case*

Calculation was performed using the acoustic module of Comsol which solves the following equation: Calculation was performed using the acoustic module of Comsol which solves the following equation:

$$\nabla \cdot \left( \frac{1}{\rho} \nabla p \right) + \frac{1}{\rho c^2} \omega^2 p = 0, \quad (19)$$

with  $p$  the acoustic pressure,  $\rho$  the mass density and  $c$  the velocity. In fact, one could have alternatively introduced the bulk modulus  $B = \rho c^2$  to describe the medium. However since we address here the wave community we find it more natural to consider medium density and wave velocity as parameters. We also stress that this acoustic module does not take into account the effect of material losses. Upon inspection of equation 1 we have:

$$\begin{aligned} \rho &= a^{-1} \\ c &= \sqrt{\frac{a}{b}} \end{aligned} \quad (20)$$

We perform a study in the frequency domain and stress that the developed theory holds so long as the wavelength is large in comparison with the dimensions

of the elementary cell. We consider a 2D problem as the geometrical transformation is 2D. Boundary conditions at left-most and right-most extremities of the medium are absorbing layers (Perfectly Matched Layers, PMLs) to mimic an infinite medium in x direction of wave propagation. In the y direction we implement periodic boundary conditions to mimic an infinite medium in y direction. We can now use the entire method described above to design an invisibility cloak for acoustic wave propagating in water ( $\rho_0 = 1000kg/m^3, c_0 = 1500m/s$ ) for example. To show the generality of the method we assume that  $a$  and  $b$  can take any value. It is of course not the case in practice (we do not have a full control of the spatial variation of velocity for example) but depending on the tuning parameters approximations are possible. One of the compromises made is due to the fact that we have an extra degree of freedom on the choice of the parameters  $(b_0, b_1)$  which are not entirely defined by the system 13. Thus we can use this extra degree of freedom to tune the velocity in order to approach more realistic materials. We consider the geometrical transformation (3) with  $R_1 = 0.05$  and  $R_2 = 0.15$ . The anisotropic inhomogeneous medium is first divided into 20 anisotropic homogeneous media. Properties of each of these anisotropic media are mimicked by using two homogeneous isotropic media and the relation (11). Elementary cells, defined by the alternation of two homogeneous isotropic media, are repeated 3 times in each anisotropic homogeneous concentric layer along the radial direction. In summary the cloak is made of 40 different media, each of them repeated three times for an overall structure consisting of an alternation of 120 homogeneous isotropic rings. Complete design of the cloak is shown in figure 5a and values of the media parameters are given in table A.2. We stress that the extreme values of the elastic parameters are needed here for a cloak of very high efficiency. As a comparison we show in table A.1 values needed for a cloak made of  $M = 5$  layers, which are more realistic in terms of existing media. An example numerical result is shown in figure 5b for a frequency of 15kHz although we stress that this design is available for any frequency providing the size of an elementary cell is small in comparison to the wavelength.

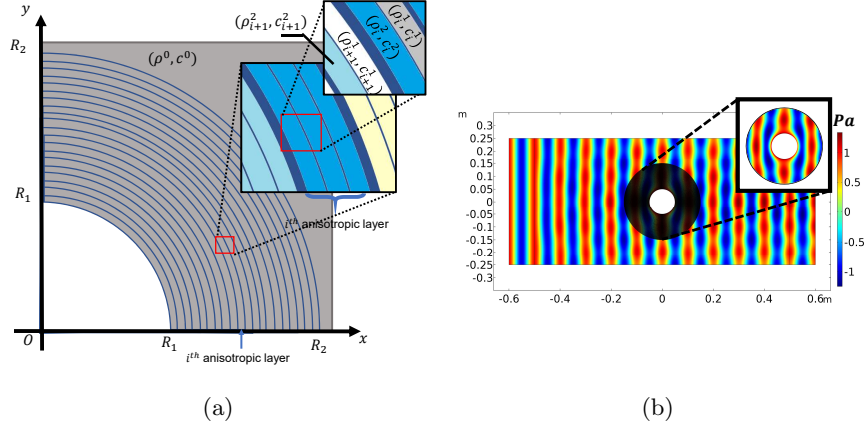


Figure 5: a) Schematic of a 1D laminar lattice made of  $M = 20$  anisotropic homogeneous media, each of them consisting of 3 alternations of homogeneous isotropic media. In total, the cloak is made of 120 alternations of homogeneous isotropic rings made of 40 different media. b) Numerical result: Propagation of a monochromatic acoustic wave of frequency  $f = 15$  kHz through the homogenized cloak designed using the 1D laminar lattice, surrounded by water. We observe that the process of inverse homogenization we developed allows us to mimic properly the inhomogeneous anisotropic medium introduced through geometrical transformation, using only homogeneous isotropic media.

#### 165 4.3. 2D rectangular lattice

In a similar way we can work out a design using a different microstructure. In the following we still consider propagation of a pressure wave in water for the non transformed part of propagation medium. The transformed medium is composed of several concentric media with rigid elliptical-like perforations. Once again the elliptical-like perforations are designed in  $(r, \theta)$  coordinates and then mapped onto  $(x, y)$  coordinates using the conformal map introduced in equation (18). Perforation shape is obtained using the genetic algorithm. The stopping criterion is a relative error of less than 5%, meaning  $\gamma(\alpha^H) < 0.05$  with input parameters identical to those introduced in figure 2b. Output parameters given by the GA for different layers are summarized in table A.3 and the geometry of the cloak is displayed in figure 6a. A qualitative numerical result is

shown in figure 6b for a representative frequency  $f = 13kHz$ . When comparing tables A.3 and A.2 we notice that the rectangular lattice is less demanding with respect to changes in mass density and velocity. In fact, mass density for the laminar lattice goes from  $47kg/m^3$  to  $21466kg/m^3$ , which seems unachievable in practice, whereas in the rectangular lattice case it goes from  $37kg/m^3$  to  $717kg/m^3$ . A similar observation can be done for velocity (from 831 m/s to 4654 m/s in laminar case, from 1495 m/s to 4734 m/s for rectangular case). When considering an experimental realization the rectangular lattice would then be more appropriate.

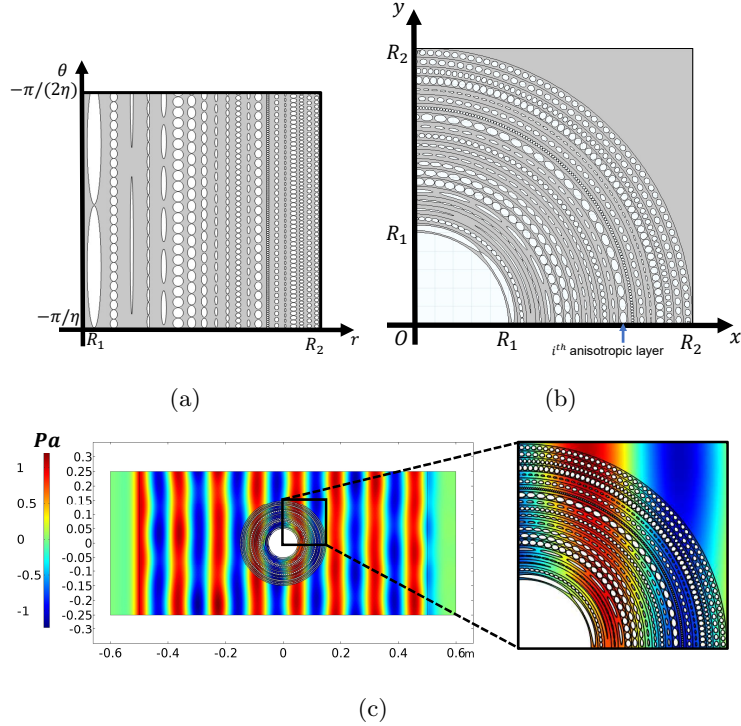


Figure 6: a) Design of the microstructure of the cloak in  $(r, \theta)$  domain, before the application of the conformal map defined by equation (18). b) Design of the microstructure of the cloak in  $(x, y)$  domain, after the conformal mapping. c) Numerical result: propagation of a monochromatic acoustic wave of frequency  $f = 13$  kHz through the homogenized cloak designed with the 2D rectangular lattice, and surrounded by water. Once again we mimic properly the inhomogeneous anisotropic medium introduced through geometrical transformation.

#### 4.4. Quantitative measure of the efficiency of the cloaks

In this section we describe the quantitative method that we choose to measure the efficiency of the cloaks depending on the frequency. To do so we compare the value of the total pressure field between homogeneous and transformed cases under study at over 5000 points located outside the region of the cloak. At a given point, we perform a ratio between the two field values (see figure 7) and we further average all the ratios. We repeat this procedure for each frequency. Obviously the closer the ratio to 1 the better the efficiency of the cloak. To complete the study we also consider an efficiency criterion defined by

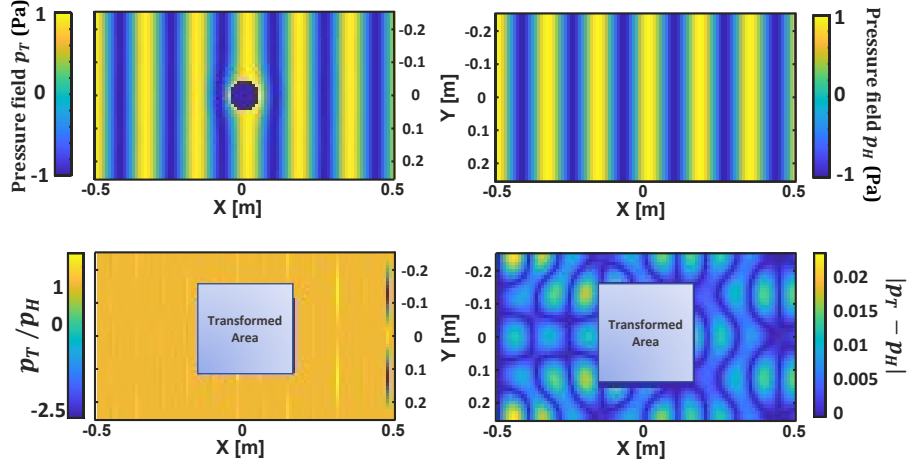


Figure 7: Illustration of procedures followed to measure efficiency. First the pressure field in the transformed medium (upper left) is divided by same in the reference homogeneous medium (upper right). The result (bottom left) expresses the cloak efficiency at each points for a given frequency ( $f = 8800$  Hz here). The closer the ratios to 1 the better the cloak efficiency. We then average the ratios computed at each point to obtain the overall efficiency at one frequency, and repeat this procedure for each frequency. We stress that due to resonance phenomena, meshing approximation or numerical approximation (for value very close to zero) artifacts can appear as we can see here on the rightmost side of the bottom left figure. The second criterion performs the difference between transformed and homogeneous media, the result is shown in the bottom left panel of the figure. We can already observe that this criterion smooths out the artifacts and reveals some resonance pattern.

the difference between the two fields which is such that the closer the difference to 0 the better the efficiency.

As a benchmark we use the anisotropic inhomogeneous cloak presented in figure 1d (ie the transformed medium without any approximation). We then compare the homogeneous case with the case introduced in figure 4 for  $M = 0$  in order to show the impact of the various cloak designs. We then compare the 1D laminar case (fig5) and the 2D rectangular lattice (fig6) against these two benchmarks. All the results are summarized in figure 8a. It should be noted that the black curve should in theory be equal to 1 at every frequency. However, with

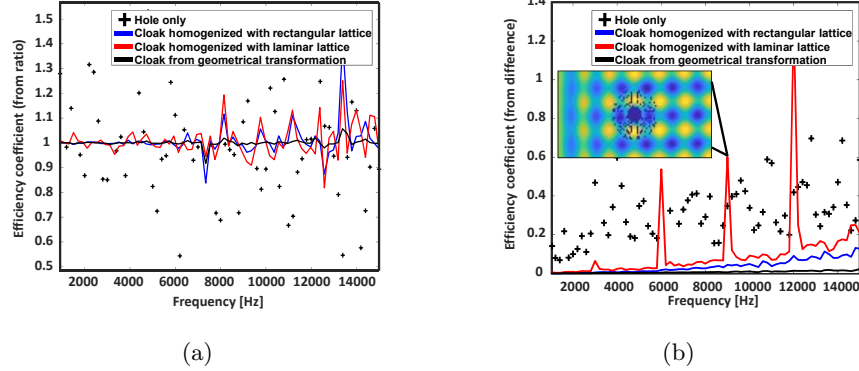


Figure 8: The crosses show the value in the case without cloak (for comparison) as shown in figure 4, the black line is the anisotropic cloak given by the transformation (figure 1d), the blue line the cloak homogenized with the rectangular lattice, the red line the cloak homogenized with the laminar lattice. a) Quantitative measure of the efficiency of each cloak for a large band of frequencies with a difference criterion defined by the ratio between the transformed case and the homogeneous case. A ratio close to one indicates a strong efficiency. b) Quantitative measure of the efficiency of each cloak for a large band of frequencies with a difference criterion defined by the difference between the transformed case and the homogeneous case. A ratio close to zero indicates a strong efficiency.

the chosen criterion singularities can occur due to vanishing denominator. Thus we give an alternative criterion in figure 8b replacing a ratio by a difference. This has the advantage of removing the imperfections of the reference curve but can none the less hide meaningful observations on cloak's efficiency.

210

We observe from these quantitative results that the efficiency of all cloaks is extremely satisfactory on the low frequency range, but this efficiency decreases at higher frequencies for the homogenized cloaks (blue and red lines). We also note that the efficiency of the cloak made of a 2D rectangular lattice decreases  
 215 faster than the 1D laminar case. This can be attributed to the fact that the elementary cells are smaller for the 1D laminar ( 0.8mm) case than for the 2D rectangular lattice (5 mm), and moreover in the 2D case the Neumann (rigid) inclusions can introduce multiple scattering. Furthermore if we look at the results given by the second criterion we observe the presence of resonant modes

220 for the perforated medium that do not appear in the other cases. If the 2D rectangular lattice seems easier to reproduce in practice, one should also take into account the loss of efficiency due to the presence of resonant modes and the faster decrease in efficiency for higher frequency.

## 5. Additional micro-structures with exotic elementary cell

225 To challenge the efficiency of the method, we further design several microstructures with more exotic elementary cells. The first one to consider is a microstructure consisting of split ring resonators as in [28], which seems to be both appropriate to obtain strong anisotropy, and also is reminiscent of the design of the first electromagnetic cloak [29]. The elementary cell of this structure and its geometric parameters are introduced in figure 9. We note that this  
230 elementary cell is defined by 9 parameters, whereas the elementary cell with an elliptic perforation was defined by 6 parameters only (and the elementary cell for homogeneous layers required only 4 parameters). Thus, it seems to us that the genetic algorithm is absolutely necessary in the present case. The resulting  
235 microstructure before and after the conformal map is shown on figure 9 and all the geometrical and physical parameters are summarized in table A.4.

We then perform numerical simulations of this microstructure. The result for one frequency and the efficiency curves for both criteria (ratio and difference between pressure fields in homogeneous and microstructured media, respectively)  
240 are shown on figure 10. We observe from the reading of figure 10 and figure 8 that the overall cloak's efficiency is not as good as for the previous microstructures which we studied. This can be attributed to the form of the inclusions that are more prone to collective resonant behavior. As we have seen before for the elliptic microstructure, resonance phenomena decrease the efficiency of the  
245 cloak. In actuality, upon inspection of figure 10b, it can be seen that the cloak only functions properly at frequencies lower than 7000 Hz (and similarly for figure 8a): clearly, the homogenization theory breaks down at frequencies above 7000 Hz. The worsening of the cloak efficiency in the split ring case can be

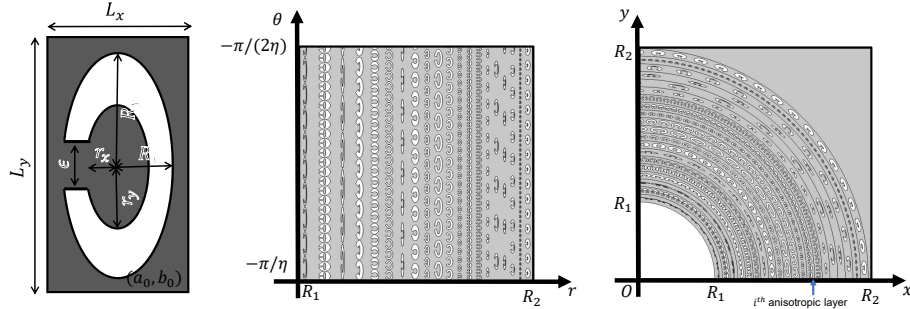
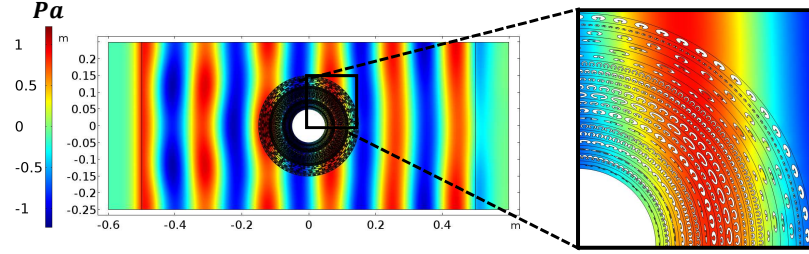


Figure 9: Left panel: the elementary cell, defined by 9 parameters. Middle panel: the microstructure before the conformal mapping,  $\eta$  is defined in equation (18). Right panel: the microstructure after the conformal mapping.

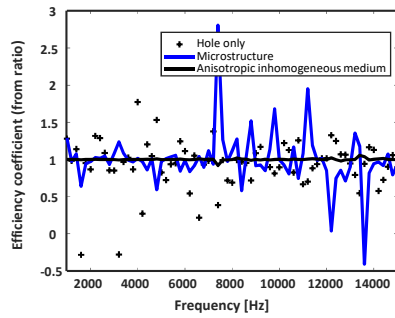
easily explained by the fact that the homogenization method which we consider  
 250 here does not take into account local resonance phenomena, thus the elementary  
 cells mimic properly the transformed medium at all frequencies except for the  
 resonant ones, as long as the ratio of unit cell size to wave wavelength remains  
 small enough.

We continue to challenge our method with a new design of elementary cell  
 255 defined again by 9 parameters. We choose this design as it seems unlikely an  
 effective medium approach could be applied to the Celtic cross within the el-  
 elementary cell (shown on figure 11): we call it a Celtic cross elementary cell.  
 Once again the elementary cell is defined by 9 parameters. We display the mi-  
 crostructured design before and after the geometric transformation on figure 11.  
 260 All the parameters of this microstructure are summarized in table A.5.

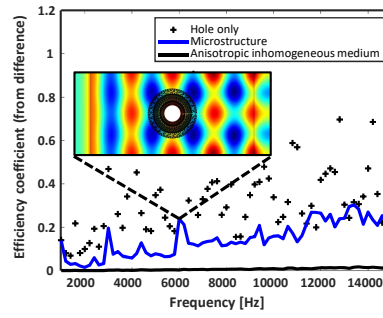
We again perform numerical simulations on this microstructure and determine  
 the efficiency curves depending on the frequency. We show the results on figure  
 12. We observe that the qualitative and quantitative results decline in com-  
 parison with our previous designs. On the positive side, we observe that the  
 265 cloak does not produce any reflections (see leftmost side of figure 12a and red  
 curves in figures 12b,12c). On the negative side, the wavefront is more distorted  
 after the cloak than it used to be in the previous designs, so the overall cloak's  
 efficiency worsens. The poor cloaking efficiency can be explained by the fact



(a)



(b)



(c)

Figure 10: a) Numerical result at a given frequency ( $f = 8000$  Hz) . b) Quantitative efficiency obtained with the ratio criterion. c) Quantitative efficiency obtained with the difference criterion. We can observe the drop in the efficiency attributed to the resonance phenomena.

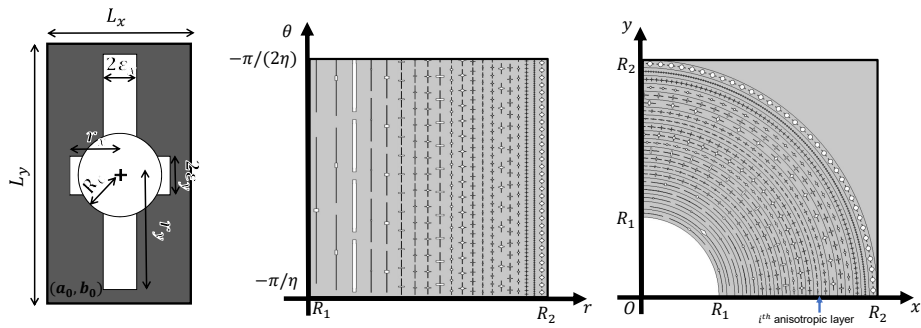
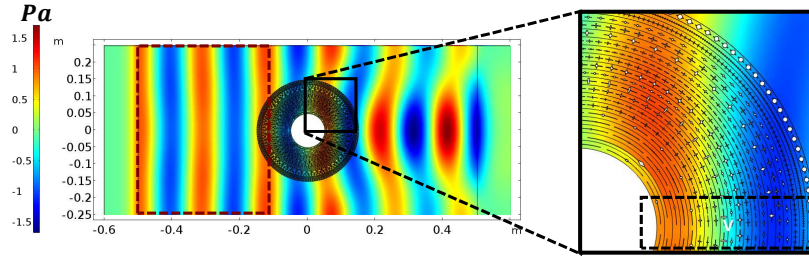
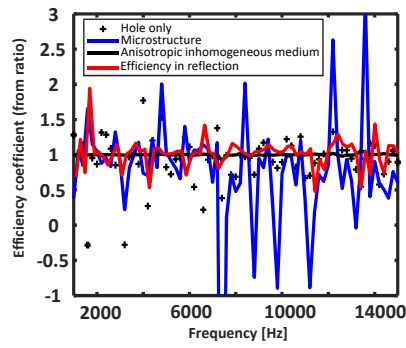


Figure 11: Left panel: the elementary cell, defined by 9 parameters. Middle panel: the microstructure before the conformal mapping. Right panel: the microstructure after the conformal mapping, see Eq. (18), where the parameter  $\eta$  is defined.

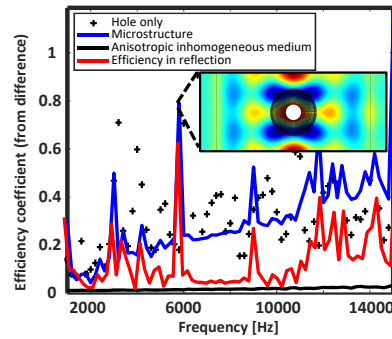
that the perimeters of the various circular homogeneous anisotropic layers are  
270 not an integer multiple of the associated elementary cells, as can be observed  
in the inset showing a magnified view in figure 12a. The salient consequence is  
a default in the microstructure. This default was also present in the previous  
design but had less influence. By comparing the qualitative result of figure 12a  
and the qualitative result in the case with no cloak (see figure 4, upper right)  
275 we still observe a clear reduction of scattering due to the cloak.



(a)



(b)



(c)

Figure 12: a) Numerical result at a given frequency ( $f = 8000$  Hz). Looking at the zoom on the microstructure we observe some design imperfections as the perimeters of the layers are not a multiple of the size of the associated elementary cell. The left part of the design being not influenced by the design imperfections the cloak does not produce any reflections. The right part introduces a distortion in the wavefront as it contains the imperfections. b) Quantitative efficiency obtained with the ratio criterion. c) Quantitative efficiency obtained with the difference criterion. We observe the drop in the efficiency attributed to the resonance phenomena and the imperfections in the microstructure.

## 6. Concluding remarks

In this paper we describe a general method to mimic complex anisotropic inhomogeneous media obtained through geometrical transformation using classical homogenization results combined with a genetic algorithm in the case of the Helmholtz equation. First the complex medium is created mathematically using the form invariance property of the Helmholtz equation, then this theoretical material is approximated by performing what we call inverse homogenization as a reference to [20]. This method can be easily adapted to several areas of wave physics such as acoustics or electromagnetism, where governing equations are form invariant. A notable constraint is that one cannot use the conformal mapping for 3D cloaks, and thus the mapping in Eq. (18), would need to be replaced by another, more complicated, one [30]. Indeed, in dimension 3, the desired conformal map should be a compound transform deduced from a homothetic transformation, an isometry and a special conformal transform (the latter being the composition of a reflection and the inversion of a sphere, such as a Moebius transform).

Our method would require further generalization to tackle elasticity cases, for which the form invariance of the governing equations is less obvious [31, 32, 33]. Considering the versatility and the room for further improvement of our method (e.g. multiphase/multiscale media and 3D designs), we believe that our approach will pave the way to further numerical studies as well as foster efforts into experimental realizations.

## References

- [1] E. J. Post, *Formal Structure of Electromagnetics : General Covariance and Electromagnetics*, Courier Corporation, 1962 (1962).
- [2] A. Nicolet, J. Remacle, B. Meys, A. Genon, W. Legros, Transformation methods in computational electromagnetism, *Journal of Applied Physics* 75 (10) (1994) 6036–6038 (May 1994). doi:10.1063/1.355500.

- [3] A. J. Ward, J. B. Pendry, Refraction and geometry in Maxwell's equations, *J. Mod. Opt* 43 (4) (1996) 773 – 793 (1996).  
305
- [4] A. Greenleaf, M. Lassas, G. Uhlmann, Anisotropic conductivities that cannot be detected by EIT, *Physiological Measurement* 24 (2) (2003) 413–419 (Apr. 2003). doi:10.1088/0967-3334/24/2/353.
- [5] U. Leonhardt, Optical conformal mapping, *Science* 312 (5781) (2006) 1777–  
310 1780 (2006).
- [6] J. B. Pendry, D. Schurig, D. R. Smith, Controlling electromagnetic fields, *Science* 312 (5781) (2006) 1780–1782 (2006).
- [7] S. A. Cummer, D. Schurig, One path to acoustic cloaking, *New Journal of Physics* 9 (3) (2007) 45 (2007).
- [8] H. Chen, C. T. Chan, Acoustic cloaking in three dimensions using acoustic  
315 metamaterials, *Applied physics letters* 91 (18) (2007) 183518 (2007).
- [9] S. A. Cummer, B.-I. Popa, D. Schurig, D. R. Smith, J. Pendry, M. Rahm, A. Starr, Scattering theory derivation of a 3d acoustic cloaking shell, *Physical review letters* 100 (2) (2008) 024301 (2008).
- [10] G. W. Milton, J. R. Willis, On modifications of Newton's second law  
320 and linear continuum elastodynamics, *Proceedings of the Royal Society A: Mathematical, Physical and Engineering Sciences* 463 (2079) (2007) 855–880 (2007).
- [11] J. Mei, Z. Liu, W. Wen, P. Sheng, Effective dynamic mass density of composites, *Physical Review B* 76 (13) (2007) 134205 (2007).  
325
- [12] D. Torrent, J. Sánchez-Dehesa, Acoustic cloaking in two dimensions: a feasible approach, *New Journal of Physics* 10 (6) (2008) 063015 (2008).
- [13] S. Guenneau, A. Movchan, F. Zolla, N. Movchan, A. Nicolet, Acoustic band gaps in arrays of neutral inclusions, *Journal of Computational and Applied  
330 Mathematics* 234 (6) (2010) 1962–1969 (2010).

- [14] M. Farhat, S. Enoch, S. Guenneau, A. B. Movchan, Broadband cylindrical acoustic cloak for linear surface waves in a fluid, *Physical review letters* 101 (13) (2008) 134501 (2008).
- [15] A. Maurel, S. Félix, J.-F. Mercier, Enhanced transmission through gratings: Structural and geometrical effects, *Physical Review B* 88 (11) (2013) 115416 (2013).  
335
- [16] G. Dupont, S. Guenneau, O. Kimmoun, B. Molin, S. Enoch, Cloaking a vertical cylinder via homogenization in the mild-slope equation, *Journal of Fluid Mechanics* 796 (-) (2016) – (2016).
- [17] A. N. Norris, Acoustic cloaking theory, *Proceedings of the Royal Society A: Mathematical, Physical and Engineering Sciences* 464 (2097) (2008) 2411–2434 (2008).  
340
- [18] D. Torrent, J. Sánchez-Dehesa, Effective parameters of clusters of cylinders embedded in a nonviscous fluid or gas, *Physical Review B* 74 (22) (2006) 224305 (2006).  
345
- [19] D. R. Smith, D. C. Vier, T. Koschny, C. M. Soukoulis, Electromagnetic parameter retrieval from inhomogeneous metamaterials, *Physical review E* 71 (3) (2005) 036617 (2005).
- [20] E. Cherkaev, Inverse homogenization for evaluation of effective properties of a mixture, *Inverse Problems* 17 (4) (2001) 1203–1218 (Jul. 2001). doi : 10.1088/0266-5611/17/4/341.  
350
- [21] V. Fokin, M. Ambati, C. Sun, X. Zhang, Method for retrieving effective properties of locally resonant acoustic metamaterials, *Physical review B* 76 (14) (2007) 144302 (2007).
- [22] A. Bensoussan, J.-L. Lions, G. Papanicolaou, *Asymptotic Analysis for Periodic Structures*, American Mathematical Soc., 1978 (Oct. 1978).  
355

- [23] D. Petiteau, S. Guenneau, M. Bellieud, M. Zerrad, C. Amra, Spectral effectiveness of engineered thermal cloaks in the frequency regime, *Scientific Reports* 4 (2014) 7386 (Dec. 2014). doi:10.1038/srep07386.
- 360 [24] W. Rowley, W. Parnell, I. Abrahams, S. Voisey, J. Lamb, N. Etaix, Deepening subwavelength acoustic resonance via metamaterials with universal broadband elliptical microstructure, *Applied Physics Letters* 112 (25) (2018) 251902 (2018).
- [25] D. Joyce, W. Parnell, R. Assier, I. Abrahams, An integral equation method  
365 for the homogenization of unidi-rectional fibre-reinforced media; antiplane elasticity and otherpotential problems, *Proceedings of the Royal Society A* 473 (2201) (2017) 20170080 (2017).
- [26] G. W. Milton, *The Theory of Composites*, Cambridge University Press, 2002 (May 2002).
- 370 [27] R. L. Haupt, S. E. Haupt, *Practical Genetic Algorithms*, John Wiley & Sons, 2004 (Jul. 2004).
- [28] J. B. Pendry, A. J. Holden, D. J. Robbins, W. J. Stewart, Magnetism from conductors and enhanced nonlinear phenomena, *Ieee Trans. Microw. Theory Tech* 47 (11) (1999) 2075–2084 (1999).
- 375 [29] D. Schurig, J. J. Mock, B. J. Justice, S. A. Cummer, J. B. Pendry, A. F. Starr, D. R. Smith, Metamaterial electromagnetic cloak at microwave frequencies, *Science* 314 (5801) (2006) 977–980 (2006).
- [30] P. Francesco, P. Mathieu, D. S en echal, *Conformal field theory*, Springer Science & Business Media, 1997 (1997).
- 380 [31] A. N. Norris, A. L. Shuvalov, Elastic cloaking theory, *Wave Motion* 48 (6) (2011) 525–538 (2011).
- [32] L. Pomot, S. Bourgeois, C. Payan, M. Remillieux, S. Guenneau, On form invariance of the Kirchhoff-Love plate equation, *arXiv preprint arXiv:1901.00067* (2019).

- <sup>385</sup> [33] D. J. Colquitt, M. Brun, M. Gei, A. B. Movchan, N. V. Movchan, I. S. Jones, Transformation elastodynamics and cloaking for flexural waves, *Journal of the Mechanics and Physics of Solids* 72 (-) (2014) 131–143 (2014).

**Appendix A. Tables of parameters for the various microstructures**

$i^{th}$ layer	$\rho_i^1$ [kg/m <sup>3</sup> ]	$c_i^1$ [m/s]	$\rho_i^2$ [kg/m <sup>3</sup> ]	$c_i^2$ [m/s]
1 ( $r = R_1$ )	6389	559	156	3575
2	2942	824	340	2426
3	2215	950	451	2105
4	1891	1028	528	1945
5 ( $r = R_2$ )	1706	1083	586	1847

Table A.1: Numerical values of the mass density and velocity used in the design of a cloak made of 5 homogeneous anisotropic layers, each of them made of 3 alternations of two homogeneous isotropic layers.

$i^{th}$ layer	$\rho_i^1$ [kg/m <sup>3</sup> ]	$c_i^1$ [m/s]	$\rho_i^2$ [kg/m <sup>3</sup> ]	$c_i^2$ [m/s]
1 ( $r = R_1$ )	21466	2261	47	4654
2	8080	2145	124	2881
3	5369	2034	186	2371
4	4193	1930	238	2117
5	3531	1831	283	1964
6	3104	1737	322	1864
7	2805	1648	356	1797
8	2582	1563	387	1752
9	2411	1483	415	1724
10	2274	1407	440	1710
11	2162	1335	462	1709
12	2069	1266	483	1721
13	1990	1201	502	1747
14	1922	1140	520	1791
15	1863	1081	537	1856
16	1811	1026	552	1952
17	1766	973	566	2096
18	1725	923	580	2323
19	1689	876	592	2722
20 ( $r = R_2$ )	831	1099	604	3639

Table A.2: Numerical values of the mass density and velocity used in the design of the cloak introduced in figure 5.

$i^{th}$ layer	$\rho_i$ [kg/m <sup>3</sup> ]	$c_i$ [m/s]	$L_x^i$ [mm]	$L_y^i$ [mm]	$r_x^i$ [mm]	$r_y^i$ [mm]
1 ( $r = R_1$ )	37	4734	8.7	76.9	2.9	38
2	182	2623	7.9	5.9	1.5	2.9
3	338	2156	7.3	103.7	0.7	42.8
4	422	1919	6.7	8.3	0.6	3.9
5	376	1912	6.3	25.9	1.1	10.7
6	205	1944	5.9	6.6	2.2	3.1
7	298	1782	5.5	7.3	1.7	3.4
8	414	1701	5.2	6.8	1.2	3
9	597	1588	4.9	7	0.6	2.7
10	548	1604	4.7	4.3	0.7	1.8
11	473	1592	4.4	3.3	1.1	1.4
12	625	1544	4.2	6.4	0.6	2.2
13	306	1686	4	5.9	1.5	2.6
14	608	1519	3.9	1.2	0.6	0.5
15	548	1535	3.7	3.8	0.9	1.4
16	717	1495	3.6	3.3	0.3	1.1
17	260	1736	3.4	2.7	1.4	1.2
18	468	1574	3.3	2.2	0.9	0.8
19	480	1564	3.2	3.2	0.9	1.2
20 ( $r = R_2$ )	446	1605	3.1	2.7	0.9	1.1

Table A.3: Numerical values of the mass density, velocity and parameters of the elementary cells used in the design of the cloak introduced in figure 6. The comparison with table A.2 show that the rectangular lattice would be experimentally less demanding than the laminar lattice.

$i^{th}$ layer	$\rho_i$ [kg/m <sup>3</sup> ]	$c_i$ [m/s]	$L_x^i$ [mm]	$L_y^i$ [mm]	$R_x^i$ [mm]	$R_y^i$ [mm]	$\epsilon^i$	$r_x^i$ [mm]	$r_y^i$ [mm]
2	137	3664	7.9	5.6	2.4	2.8	2.9	0.5	2.1
3	320	2458	7.3	21.8	0.7	10.5	3.6	0.3	6.2
4	313	2485	6.7	11.9	1.7	5.7	4.5	0.3	2.6
5	292	2451	6.3	6.8	1.8	3.2	2.1	1.2	1.3
6	349	2193	5.9	6.1	1.6	2.9	2	0.9	2
7	572	1832	5.5	18.1	0.6	6.9	5.4	0.5	2.4
8	380	2214	5.2	11.2	1.6	4.6	2	0.8	1.6
9	501	1951	4.9	7.2	1.1	2.8	1.4	0.3	1.7
10	321	2308	4.7	12.4	1.7	5.2	2.2	0.7	3.7
11	409	2104	4.4	7.3	1.5	3	2.8	0.5	2
12	571	1828	4.2	4.9	0.8	1.9	0.8	0.3	0.9
13	490	2002	4.0	3.6	1.1	1.4	0.9	0.1	1.1
14	468	1918	3.9	3.6	1.2	1.4	1.3	0.6	1
15	722	1655	3.7	9.9	0.5	2.6	1.7	0.2	0.6
16	699	1621	3.6	22.5	0.9	4.7	3.7	0.7	3
17	750	1611	3.4	21.1	0.5	4.2	1.8	0.4	1.8
18	655	1675	3.3	12.9	0.9	3.2	2.8	0.7	1.7
19	761	1598	3.2	2.8	0.3	0.9	0.5	0.2	0.4
20 ( $r = R_2$ )	511	1965	3.1	8.7	0.1	2.8	1.2	0.1	1.1

Table A.4: Numerical values of the mass density, velocity and parameters of the elementary cells used in the design of the cloak introduced in figure 9

$i^{th}$ layer	$\rho_i$ [kg/m <sup>3</sup> ]	$c_i$ [m/s]	$L_x^i$ [mm]	$L_y^i$ [mm]	$r_x^i$ [mm]	$r_y^i$ [mm]	$\epsilon_x^i$ [mm]	$\epsilon_y^i$ [mm]	$R_c$
1 ( $r = R_1$ )	107	3990	8.7	56.8	0.9	24.6	0.08	1.3	1
2	248	2537	6.3	142.7	0.9	61.3	0.07	3.5	1.8
3	379	2231	7.3	37.3	0.3	16.1	0.06	0.5	0.7
4	449	2051	6.7	28.2	0.3	12.1	0.12	0.3	0.3
5	488	1814	6.3	27.2	0.9	11.6	0.08	0.7	0.8
6	520	1664	5.9	10.5	1.2	4.5	0.08	0.3	0.3
7	621	1633	5.5	9.1	0.7	3.8	0.05	0.1	0.4
8	577	1549	5.2	9.1	1.3	3.6	0.1	0.2	0.5
9	536	1480	4.9	13	1.7	5	0.09	0.4	0.5
10	675	1586	4.7	5.9	0.6	2.2	0.05	0.1	0.6
11	563	1428	4.4	8.5	1.6	3.3	0.12	0.1	0.7
12	666	1455	4.2	5.4	1	2.1	0.09	0.03	0.3
13	788	1538	4	4.1	0.2	1.5	0.07	0.02	0.3
14	733	1468	3.9	4.5	0.7	1.6	0.05	0.1	0.3
15	685	1459	3.7	11.1	1.2	3	0.06	0.3	0.7
16	690	1442	3.6	6.6	1	2.1	0.09	0.2	0.3
17	826	1437	3.4	5.4	0.6	1.5	0.04	0.04	0.4
18	678	1458	3.3	2.1	0.7	0.9	0.06	0.02	0.2
19	786	1490	3.2	1	0.3	0.4	0.02	0.05	0.2
20	560	1494	3.1	4.2	1	1.5	0.08	0.2	0.9

Table A.5: Numerical values of the mass density, velocity and parameters of the elementary cells used in the design of the cloak introduced in figure 11